Konrad-Zuse-Zentrum
für Informationstechnik Berlin

Takustraße 7
D-14195 Berlin-Dahlem
Germany

HEIKO SCHMIDT[1] MICHAEL OEVERMANN[2]
ROB J.M. BASTIAANS[3] ALAN R. KERSTEIN[4]

A priori Tabulation of Turbulent Flame Speeds via a Combination of a Stochastic Mixing Model and Flamelet Generated Manifolds, Extended to Incorporate Strain Effects

[1]Zuse Institute Berlin (ZIB),
e-mail: heischmi@math.fu-berlin.de
[2]Technische Universität Berlin, Institut für Energietechnik,
e-mail: michael.oevermann@tu-berlin.de
[3]Eindhoven University of Technology, Mechanical Engineering, The Netherlands,
e-mail: r.j.m.bastiaans@tue.nl
[4]Combustion Research Facility, Sandia National Laboratories, Livermore, CA, USA,
e-mail: arkerst@sandia.gov

The work was partially supported by the Division of Chemical Sciences, Geosciences, and Biosciences, Office of Basic Energy Sciences, United States Department of Energy, and by the National Science Foundation under Grant No. ATM-0346854.

ZIB-Report 09-09 (March 2009)

A priori Tabulation of Turbulent Flame Speeds via a Combination of a Stochastic Mixing Model and Flamelet Generated Manifolds, Extended to Incorporate Strain Effects

H. Schmidt, M. Oevermann, R.J.M. Bastiaans, and A.R. Kerstein

March 9, 2009

Abstract

In this paper we revisit the *a priori* turbulent flame speed tabulation (TFST) technique for a given parameter space within the region of flamelet combustion-regimes. It can be used as a subgrid-scale (SGS) model in Large Eddy Simulation (LES). In a first step, stationary laminar flamelets are computed and stored over the progress variable following the ideas of flamelet generated manifolds (FGM). In a second step, the incompressible one-dimensional Navier-Stokes equations supplemented by the equation for the progress variable are solved on a grid that resolves all turbulent scales. Additionally, turbulent transport is implemented via the linear eddy model (LEM). The turbulent flame structures are solved until a statistically stationary mean value of the turbulent flame speed has been reached. The results are stored in a table that could be used by large scale premixed combustion models, e.g. front tracking schemes. First results are compared quantitatively with direct numerical simulations (DNS) taken from literature. Then it is illustrated in one example how the new method could help to fix constants in algebraic models for turbulent flame speeds. Further it is shown how the technique can be extended to incorporate turbulent strain effects. Finally we investigate the effect of the use of detailed and tabulated chemistry under unsteady conditions.

Keywords: turbulent premixed combustion, flame structures, linear eddy model, flamelet generated manifolds, turbulent flame speed tabulation, strain effects

Contents

1 Introduction

Due to the interaction between many different time and length scales, turbulent premixed combustion simulation remains a challenging task. Whereas the largest turbulent scales and the slow chemical processes are resolvable, the small scale turbulence/chemistry interaction often has to be modelled. Therefore, the reactive Navier Stokes equations are filtered, dividing the original solution into resolved and unresolved parts, where the latter needs closure. This is commonly done using parameterizations that relate the unresolved parts to the resolved field. For example, the turbulent flame speed, s_t, is an important quantity [21], that is used in many approaches to premixed combustion modeling, e. g., level set methods, flame surface density models, and progress-variable type approaches [6, 22, 32]. A flame tracking scheme which resolves all length scales - a DNS solver in that sense - would resolve the complete flame surface using a laminar flame speed s_l to propagate the flame. This is often done using a level set ansatz. Nevertheless, the idea is to use these schemes when scale separation occurs and the flame structure is not fully resolved. In this case the flame area, as well as flame stretching, cannot be calculated correctly. Therefore an effective turbulent flame speed has to compensate this effect. Detailed derivations of all these effects can be found, e.g., in [21]. There are different possibilities to evaluate s_t. The simplest and perhaps least physical is a simple algebraic expression, where often s_t is a function of the turbulent velocity fluctuations u' and the laminar flame speed s_l

$$s_t = f(u', s_l). \tag{1}$$

Nowadays, the turbulent flame speed might alternatively be extracted from stand-alone computations of detailed turbulent flame structures [1, 24]. However these simulations are very expensive and can therefore not be used to span an extended parameter space. On the other hand, these detailed simulations can be used to validate alternative methods.

One of the alternative methods, more recently developed, uses so-called superparameterization to determine s_t. Here a one-dimensional microstructure evolution for turbulence chemistry interaction, e.g. [26], is forced by the resolved solution. Suitable integrals over the microstructure yield some of the needed closure terms like the turbulent flame speed. However this procedure is done "online", increasing the costs of such a computation considerably. Even for (stand-alone) one-dimensional calculations of turbulent premixed flames using detailed chemistry and the Linear Eddy Model (LEM [15]) for turbulent transport, the effort is quite high [19, 24].

In this paper, we propose a technique of a priori tabulation of s_t for a given reactive setup, e.g., geometric scales, fuel, equivalence ratio, and so on. It can be used as SGS model for LES. In order to accelerate turbulent flame computations, here the flamelet generated manifold (FGM) method [29] is applied to obtain chemical source terms and local mass fraction values. FGM can be considered as a combination of the flamelet approach and the intrinsic low dimensional manifold (ILDM) method [17] and is equivalent to the flame prolongation of ILDM, FPI, introduced in [9]. FGM is applied similarly to ILDM. However in FGM, the data base is not generated by applying quasi-steady-state relations for chemical source terms, but by solving a set of one-dimensional convection-diffusion-reaction equations to a steady state of a laminar flame structure. The

main advantage of FGM is that diffusion processes, which are important between the preheat zone and the reaction layer, are taken into account. This leads to an accurate method for premixed flames that uses fewer controlling variables than ILDM.

The potential of using FGM is that minor species can be predicted as well, e.g. NO_X emissions. Moreover the use of FGM-LEM is investigated for stretched cases in this study. This opens the potential for obtaining accurate predictions also in the thin reaction zones regime.

To put the present study in perspective a brief overview of efforts is given in the following. First extensions of Kerstein's LEM idea [15] to combustion have been proposed in literature by Menon and Kerstein [18] and improved by Smith and Menon [28]. In these studies the chemistry is described by simple kinetics using up to four reactions. However it is shown that the method has potential to capture many underlying features of a turbulent premixed flame and is capable of predicting the turbulent flame speed. In later studies by Chakravarthy and Menon [4, 5] the model was used to simulate turbulent premixed stagnation point flames. Here it is concluded that wrinkled as well as corrugated flame propagation can be handled using the method. Hewson and Kerstein [13] used a one-dimensional turbulence (ODT) model. With this model, which is argued to be more physical then LEM, some improvements are reported. However, discrepancies in mixing rates were observed between simulations and measurements. Goldin [10] proposes a constructed probability density function (PDF) model for non-premixed combustion that approximates the species and temperature at a point in a general turbulent reacting flow by the species and temperature that evolved in an independent homogeneous turbulent flow. The thermo-chemical PDF is parameterized by a suitable set of lower moments, and tabulated for retrieval in 3D CFD codes. The Linear Eddy Model is used to resolve, affordably, detailed kinetic calculations in the homogeneous turbulence geometry. In a study by Sankaran and Menon [25], exploring premixed turbulent combustion again, also the thin reaction zones regime is accessed with LEM and large-eddy simulations of statistically 1D turbulent flames are presented. The method is shown to be valid in this region, although the chemistry is approached by a one step scheme, including variable Lewis numbers for the five species.

The LEM-FGM strategy in the present paper is as follows. The s_t values for the table are computed by evolving one-dimensional turbulent flame structures to a statistically steady state. The steady state assumption is tested with unit root tests and by looking at the convergence of the mean. In the flame structure computation we use LEM for the turbulent transport and the idea of Flamelet Generated Manifolds (FGM) [29] for the chemistry tabulation. Both are linked to an implicit solver for the one-dimensional Navier-Stokes equations [14]. As long as the smallest turbulent eddies do not enter the reaction zone, (laminar) chemistry and turbulence can be treated separately. For the chemistry we apply FGM [29].

In a first step we compute steady one-dimensional laminar flamelets with detailed chemistry and tabulate the flame structure as a function of a suitable progress variables, e. g. CO_2 for a methane air mixture. Additional parameters for tabulation depending on their physical relevance could be stoichiometry, enthalpy, or flame stretch, which changes the laminar burning velocity. In DNS-FGM a correct influence of stretch on the burning velocity was found in Bastiaans et al. [2]. Here, a limited representation of stretch is proposed (see

section 6).
In the second step we solve the zero Mach number equations for mass, momentum, energy, and progress variable in a one-dimensional domain resolving all spatial and temporal scales. Turbulent advection is implemented using the stochastic LEM. Species mass fractions are uniquely determined by mapping between the progress variable and the pre-calculated FGM of step one. The calculations of step two are performed until a statistically stationary value of s_t has been reached.

Generally in a realistic setup the integral length scale is geometry dependent and is a function of space and time. Using our method together with a RANS or LES scheme, the global scheme has to provide the integral scale l_t as well as a characteristic time scale τ. In future work l_t can be easily incorporated in our tabulation as an independent variable. Our method can generate a converged time series and the PDF of s_t. The present paper shows results of the given implementation for the turbulent burning speed. These results are validated with databases from DNS studies. It is discussed how our method could help to improve currently used algebraic models. This validation is followed by an analysis of stretch effects that can be incorporated in the database. Besides this, an analysis of unsteady effects, including detailed chemistry, is provided at the end of the paper.

Thus, the paper is organized as follows. In the next section, we outline our modeling approach. In section 3 results for turbulent premixed flames for different equivalence ratios and turbulence intensities are presented. These results are compared with DNS taken from literature in section 4. In section 5 it is discussed how our method could help to improve currently used algebraic models. Further it is shown how the technique can be extended to incorporate turbulent strain effects in section 6. Finally we investigate the effect of the use of detailed and tabulated chemistry under unsteady conditions in section 7. The paper ends with conclusions on the approach and an outlook for further investigations.

2 Model Formulation

Our modeling approach consists of a combination of different stand-alone models, where each model reduces the complexity and cost of turbulent reactive multi-dimensional flow computations.

The manifold tabulated using FGM consists of all species mass fractions, temperature, and all source terms. (Tabulation of the source terms is convenient though not necessary because they can be computed from the other quantities.) The main steps are (i) constructing an FGM table by computing a sequence of laminar flames to a steady state, (ii) computing a sequence of turbulent flame structures using LEM and the FGM results from (i), (iii) extracting the turbulent burning speed for each run when convergence of the mean is reached, and (iv) building the turbulent data base.

2.1 Flamelet generated manifolds

To make the sequence of turbulent flame structure computations feasible, we apply the flamelet generated manifold (FGM) method [29] to obtain chemical source terms and local mass fraction values. The manifold used in this paper is based on a methane/air kinetic mechanism with 16 species and 36 reactions taken from [20]. The extension of the idea to more complicated mechanisms is straightforward [8].
In order to generate the manifolds in step (i), we solve the variable-density Zero-Mach-number equations in one spatial dimension on a regular grid. The balance equations for species mass fractions Y_s and temperature T are

$$\rho\frac{\partial Y_s}{\partial t} + \rho u\,\frac{\partial Y_s}{\partial x} = -\frac{\partial j_s}{\partial x} + M_s\,\dot{\omega}_s, \tag{2}$$

$$\rho c_p\frac{\partial T}{\partial t} + \rho u c_p\,\frac{\partial T}{\partial x} = -\frac{\partial q}{\partial x} - \sum_s j_s\,\frac{\partial h_s}{\partial x} - \sum_s h_s\,M_s\,\dot{\omega}_s, \tag{3}$$

with $s = 1, \ldots, n_s$. Here, ρ is the density, u the velocity, j_s the species diffusive flux, M_s the molecular weight of species s, M the mean molecular weight of the mixture, $\dot{\omega}_s$ the chemical source term of species s, c_p the heat capacity at constant pressure, p the pressure, q the heat flux, and h_s the enthalpy of species s including the heat of formation. In the zero-Mach number limit the pressure is spatially constant and we have a divergence constraint on the velocity

$$\begin{aligned}\frac{\partial u}{\partial x} = &-\frac{1}{\rho c_p T}\left\{\frac{\partial q}{\partial x} + \sum_s j_s\,\frac{\partial h_s}{\partial x}\right\} \\ &-\frac{1}{\rho}\sum_s\left\{\frac{M}{M_s}\frac{\partial j_s}{\partial x}\right\} + \frac{1}{\rho}\sum_s\left\{\frac{M}{M_s} - \frac{h_s}{c_p T}\right\} M_s\dot{\omega}_s\end{aligned} \tag{4}$$

that can be derived from total energy conservation. With a prescribed inflow velocity u_1 at the location x_1 the velocity field follows by simple integration of u in space. Here, the inflow condition is varied to balance s_t. The density is calculated from the equation of state for an ideal gas $p = \rho\,T\,\sum_s Y_s\,R_s$, where p is the prescribed and spatially constant thermodynamic pressure. The velocity u in equations (2) and (3) represents the flow velocity induced by dilatational effects due to compression, conduction, and chemical reactions as given by (4). The zero-Mach-number equations are solved numerically using standard second-order finite-difference discretizations using standard [16] upwind discretizations for convective and central difference for viscous terms. The time integration of the stiff set of equations is performed using the DAE solver IDA of the SUNDIALS package [14]. Thermodynamic and transport properties as well as reaction rates are calculated using the C++ interface of the CANTERA software package [11]. Diffusion velocities can be calculated using a mixture-based formulation with variable Lewis numbers for all species. Nevertheless, here we consider for simplicity the unity Lewis number case.

Note that we have described the general equations of incompressible reactive fluids together with a discrete solution method. Since we are considering stationary free laminar flames in step (i), a lot of simplifications can be used, e.g. that ρu is constant. Since it is a laminar flat flame, s_l is an eigenvalue of the system which can be calculated directly, and there is no need to vary the inflow

condition. However, we use the more general form, because in the next step (ii) (see next section) we will consider the turbulent flame case, where we need a converged laminar flame profile as an initial condition. Since we don't want to use two different codes for the two stages, we have written the equations in general form. Obviously, the user of our method could use more efficient strategies for the laminar flame computations in step (i) and then has to switch to a more elaborated solver for the turbulent case in step (ii).

2.2 Linear eddy mixing to simulate turbulent transport

In step (ii) of our modeling strategy we solve equation (4) together with an equation for the progress variable Y_p, here $p = CO_2$,

$$\rho\frac{\partial Y_p}{\partial t} + \rho u\,\frac{\partial Y_p}{\partial x} = -\frac{\partial j_p}{\partial x} + M_p\,\dot{\omega}_p. \tag{5}$$

The source terms $\dot{\omega_s}$ appearing in equation (4) are taken from the FGM tables via interpolation, whereas all thermodynamical properties and mixture based transport coefficients are evaluated using the CANTERA package [11] using the local mass fraction values taken from the FGM.
To extend the concept to the turbulence case we use a stochastic mixing model. In the LEM concept [15], turbulent advection is implemented explicitly by stochastic eddy events. Each eddy event involves a rearrangement of all scalar quantities using so-called 'triplet maps'. The effect of a triplet map is a three-fold compression of the scalar fields in a selected spatial interval whose size is denoted l. This map increases the scalar gradients within the selected interval, analogous to the effect of compressive strain in turbulent flow, without creating discontinuities. Three parameters are needed to implement the eddy events: eddy size l, eddy location within the domain, and the eddy event frequency. The eddy location is randomly sampled from a uniform distribution, and the eddy size is usually randomly sampled from a given size distribution (e. g., a distribution based on the Kolmogorov inertial-range scaling). The integral length scale l_t and the turbulent diffusivity D_t are the required inputs to the LEM formulation used here. D_t is determined from $D_t = C_D\,l_t u'$ with $C_D = 1/15$ taken from [19, 24, 27, 28]. Another parameter is the Kolmogorov scale η. It is determined from the turbulent Reynolds number $Re_t = u' * l_t/\nu$, where ν is the kinematic viscosity. Then the Kolmogorov scale is $\eta = N_\eta * l_t * Re_t^{-3./4.}$, where we use the constant $N_\eta = 4$ as in [19, 24, 27, 28]. It is important to note that similar to a DNS, in the LEM concept equations (2) and (3) need to resolve all spatial scales of a turbulent reacting flow.

The LEM parameters are fixed in time for a given case, corresponding to stationary turbulence, which is the basis for evaluating s_t in the present study. An interesting question that is not addressed here is whether s_t values obtained in this way are the same as values obtained in a transient turbulent flow corresponding at a given instant to the same turbulent state, based on LEM parameter values (in this case time-varying), as a stationary turbulent state used to evaluate s_t. Such an investigation would be a useful test of the concept of turbulent burning speed tabulation for premixed combustion simulation.

2.3 The turbulent burning speed

Each coupled LEM/hydrodynamic simulation yields a time series of turbulent premixed methane flame structures. The net mass burning rate is evaluated as an integral over the source terms of the progress variable

$$\rho_u s_t(t) = \frac{1}{Y_{p,x_1} - Y_{p,x_0}} \int_{x_0}^{x_1} \rho(t)\dot{\omega}_p(t)dx, \tag{6}$$

where ρ_u is the density of the unburnt mixture, x is the one-dimensional coordinate and ω_p denotes the source term of the progress variable Y_p. Hence, the outcome of each LEM run is a time series $s_t(t)$. From this series one could construct the PDF of s_t for the given turbulence level and composition. For the PDF, one has to check for strong convergence, whereas for a steady mean value and variation, only weak convergence is required. Here, we focus on the latter. Whether one has fast or slow convergence depends strongly on the underlying process. If the PDF is near Gaussian, it is reached much faster than for, e.g., burning speeds of flames in the thin reaction zone regime, where a typical PDF(s_t) is far from being Gaussian. Here, the runs are stopped when the mean converges.

In principle also statistical tests for could be used to check time series for steadiness. E.g., the so-called unit tests check time series for steadiness and can be found in software packages like e.g. the "R" Project [23] for statistical computing. Nevertheless, most of the tests for steadiness have problems with one sided PDFs and rare events as it is the case for our PDF(s_t). There are solution strategies which are far away from being standard. Therefore, even if the tests yield steadiness as a result we analyze additionally the behavior of the mean $\overline{s_t}(t)$.

3 Generating the TFST data base

In this section we give an example of how to build a data base for the turbulent flame speed that might be used later by, e.g., a level-set front-tracking scheme or any other numerical method for premixed turbulent combustion using s_t. We illustrate the main steps, namely (i) constructing a FGM table by computing a sequence of laminar flames to a steady state, (ii) computing a sequence of turbulent flame structures using LEM with a progress variable approach using the FGM results, (iii) extracting the turbulent burning speed for each run when (at least) weak statistical convergence is reached, and (iv) building the turbulent data base.

3.1 The FGM tabulation

In Figure 1 the tabulated chemical source term of the progress variable CO_2 using the chemical reaction mechanism for CH_4 combustion from Peters [20] is plotted as a function of the progress variable and equivalence ratio ranging from lean to stoichiometric conditions. The source terms of all other variables are stored as well. Some results of laminar flame properties obtained with the model are summarized in Table 1.

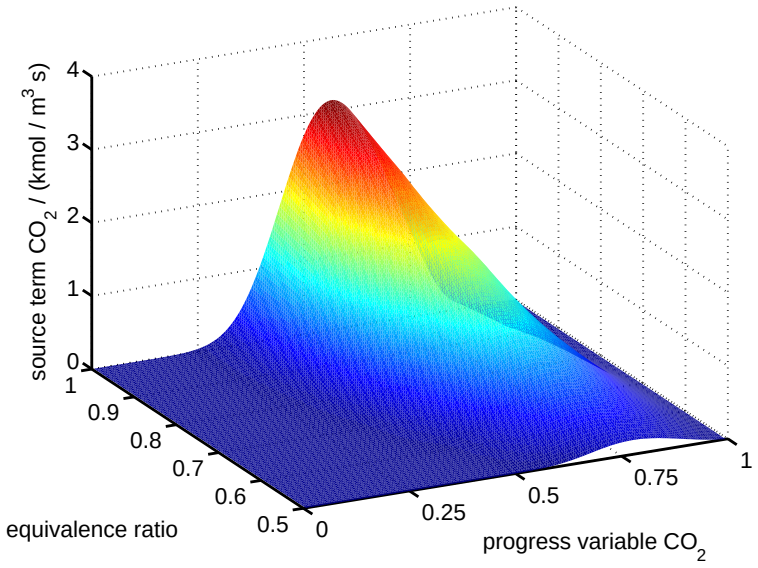

Figure 1: Tabulated source term of the progress variable, CO_2, over stoichiometry mixture using methane/air chemistry.

$\phi[-]$	0.5	0.6	0.7	0.8	0.9	1.0
l_F[mm]	1.348	0.746	0.556	0.478	0.449	0.442
s_l[m/s]	0.0657	0.1411	0.2160	0.2781	0.3197	0.3363

Table 1: Laminar flame thickness (l_F) and the laminar burning speed (s_l) for different equivalence ratios ϕ.

3.2 Turbulent flame structures

In the second step we use the FGM generated source terms as an input for the LEM computations of the turbulent flame structures. This approach reduces the number of species within the LEM module to the number of progress variables of the FGM and allows a fast computation over a large parameter space. Here we use CO_2 as progress variable. Some snapshots of a calculated turbulent methane/air flame structure for $\phi = 0.8$, $l_t = 5$mm, and $u' = 0.6$m/s are plotted in Figure 2 (main species) and Figure 3 (minor species).

3.3 The extracted turbulent burning speed and statistical convergence

From each flame structure we extract the turbulent burning speed via equation (6). A typical time history of s_t/s_l as well as its mean value as function of time is plotted in Figure 4. Time axis is normailzed by the integral eddy turn over time τ. To obtain strong statistical convergence, one has to wait until the whole PDF of s_t is converged. Here, we stop the computations when the

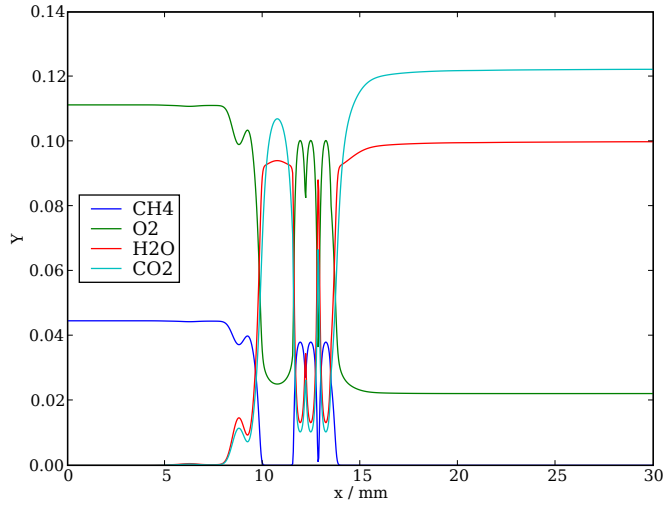

Figure 2: Snapshot of the major species of the turbulent methane flame for $\phi = 0.8$, $l_t = 5$mm, and $u' = 0.6$m/s

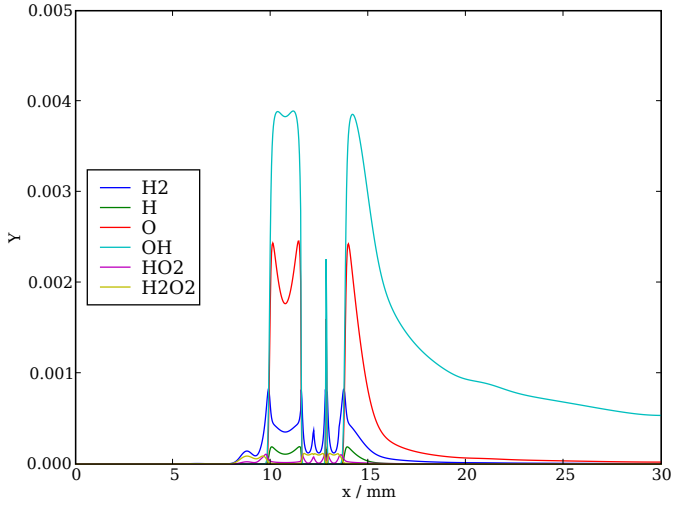

Figure 3: Snapshot of the minor species of the turbulent methane flame for $\phi = 0.8$, $l_t = 5$mm, and $u' = 0.6$m/s

first moment is converged to a steady state. This constraint is even less than is normally meant by weak statistical convergence which requires convergence of mean and variance. In Figure 5 a time history of s_t is shown for doubled turbulence intensity compared to Figure 4. It can be concluded that, even to get convergence of the mean of s_t/s_l, it is necessary to calculate over a time

interval that is quite large compared to the integral eddy turn over time. For the different set-ups, the factor ranges from about 20 to 100. Generally, this is a much longer time than standard DNS cases are run for, but DNS runs may be less intermittent compared to our LEM simulations.

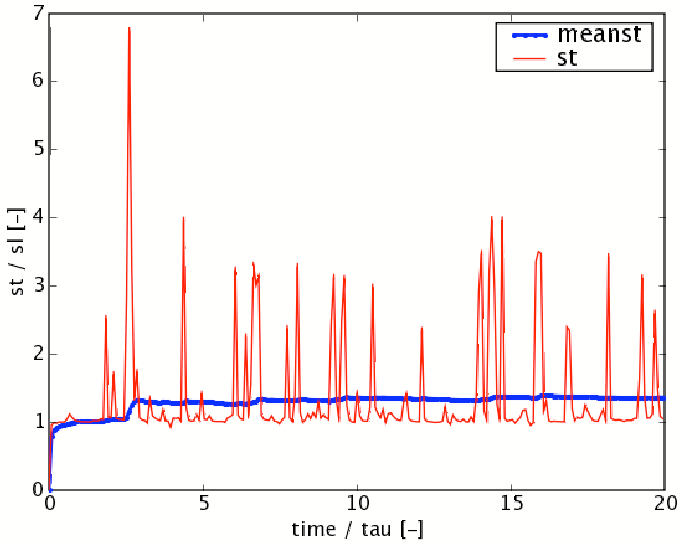

Figure 4: Time history of the turbulent burning velocity for the case $\phi = 0.7$, $l_t = 5$mm, and $u' = 0.66$m/s

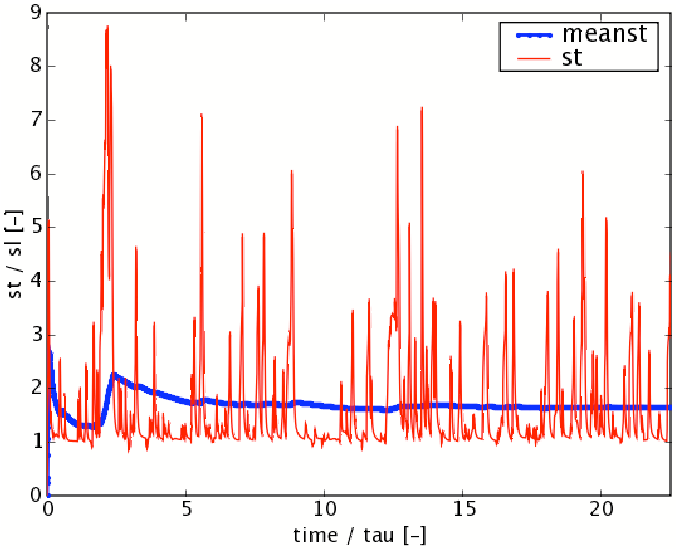

Figure 5: Time history of the turbulent burning velocity for the case $\phi = 0.7$, $l_t = 5$mm, and $u' = 1.3$m/s

To check the tabulated results we redo a calculation using detailed chemistry. A comparison of the two time evolutions for the turbulent burning velocity are

plotted in Figure 6. The comparison is quite reasonable, especially for the mean value of s_t, but a more detailed evaluation in section 7 indicates some limitations of the FGM.

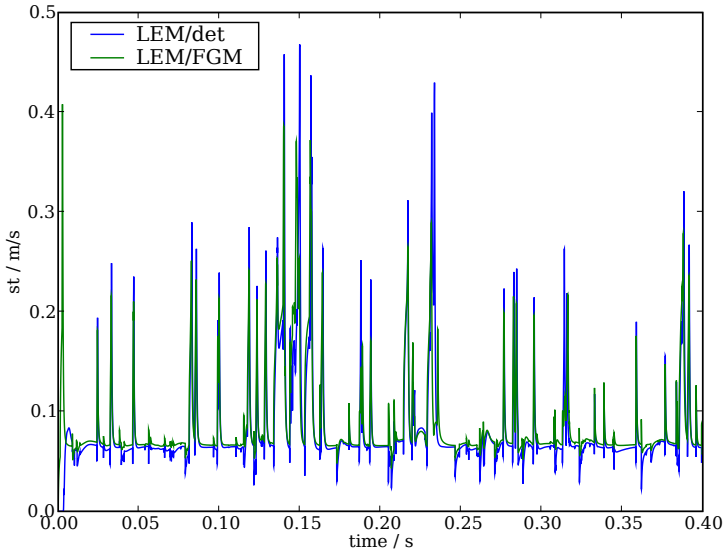

Figure 6: Time evolution of the turbulent flame speed for detailed and tabulated chemistry for the same initial conditions

3.4 The turbulent burning velocity as a function of stoichiometry and turbulent fluctuations

To construct a data base of s_t values, we repeat the turbulent flame structure computations for different turbulent fluctuations and equivalence ratios. Our tabulation region is shown in a qualitative combustion diagram, see Figure 7.

The exact coordinates of the computations which depend in our example on equivalence ratio and turbulence conditions are summarized in Table 2.

u'[m/s]\ϕ	0.5	0.6	0.7	0.8	0.9	1.0
0.33	5.02; 3.71	2.34; 6.7	1.53; 8.99	1.19; 10.46	1.03; 11.14	0.98; 11.31
0.66	10.04; 3.71	4.68; 6.7	3.06; 8.99	2.37; 10.46	2.06; 11.14	1.96; 11.31
0.99	15.07; 3.71	7.02; 6.7	4.58; 8.99	3.56; 10.46	3.10; 11.14	2.94; 11.31
1.30	19.79; 3.71	9.21; 6.7	6.02; 8.99	4.67; 10.46	4.07; 11.14	3.87; 11.31

Table 2: Coordinates (y; x) = $u'/s_l; l_t/l_F$ in Figure 7 for the cases considered

The results for the mean turbulent burning speed are shown in Table 3 and the interpolated manifold is plotted in Figure 8.

The interpolated s_t shows a monotonic behavior. Highest values are reached for the stoichiometric flame at the highest turbulence intensity. For lean mix-

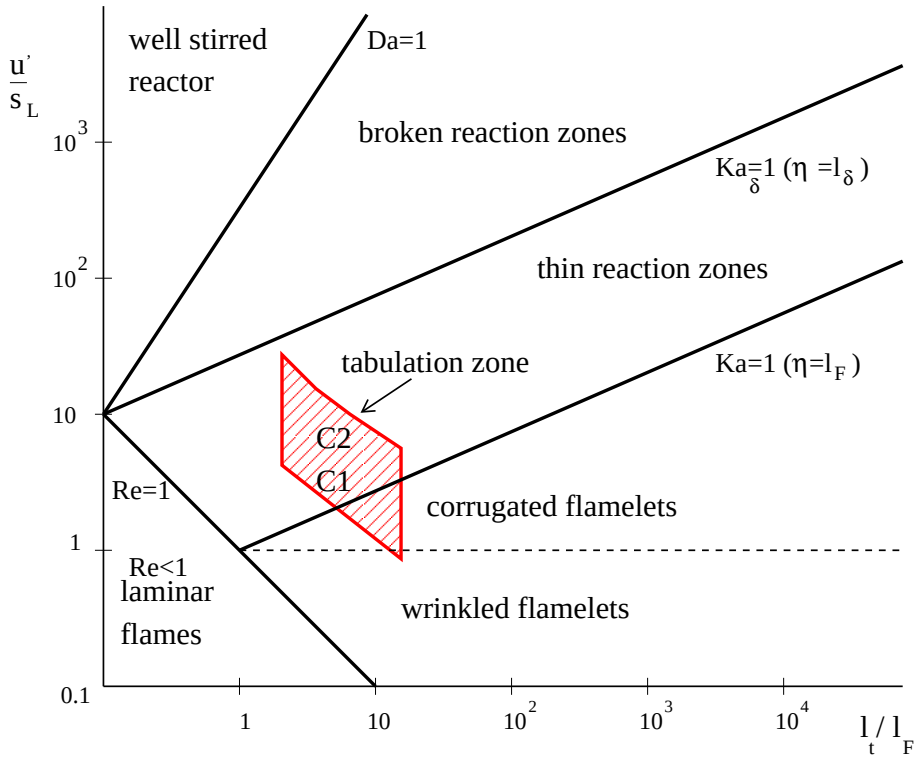

Figure 7: Diagram of turbulence/chemistry regimes. Conditions C1 and C2 are discussed in section 4

u'[m/s] \ ϕ	0.5	0.6	0.7	0.8	0.9	1.0
0.33	0.0870	0.1728	0.2645	0.3350	0.3859	0.3966
0.66	0.0914	0.2095	0.3008	0.3834	0.4253	0.4352
0.99	0.09810	0.2245	0.3407	0.4508	0.4801	0.5226
1.30	0.1097	0.2382	0.3615	0.4668	0.5372	0.5675

Table 3: The mean turbulent burning speed, s_t in $[m/s]$, as a function of stoichiometry and velocity fluctuations for the different calculations

tures changes in turbulence levels have a smaller effect than for richer flames. This can be explained by the different laminar flame thicknesses and the associated change in combustion regime.

4 Comparison with DNS results

For a first quantitative comparison we prefer to use DNS results of statistically flat flames. To that end we use two recent DNS cases, one by de Swart et al. [8] and one by Chakraborty and Cant [3]. The reason for taking such cases is that statistically flat flames might be seen as an elementary small scale building block of a turbulent premixed flame. So one is interested to investigate

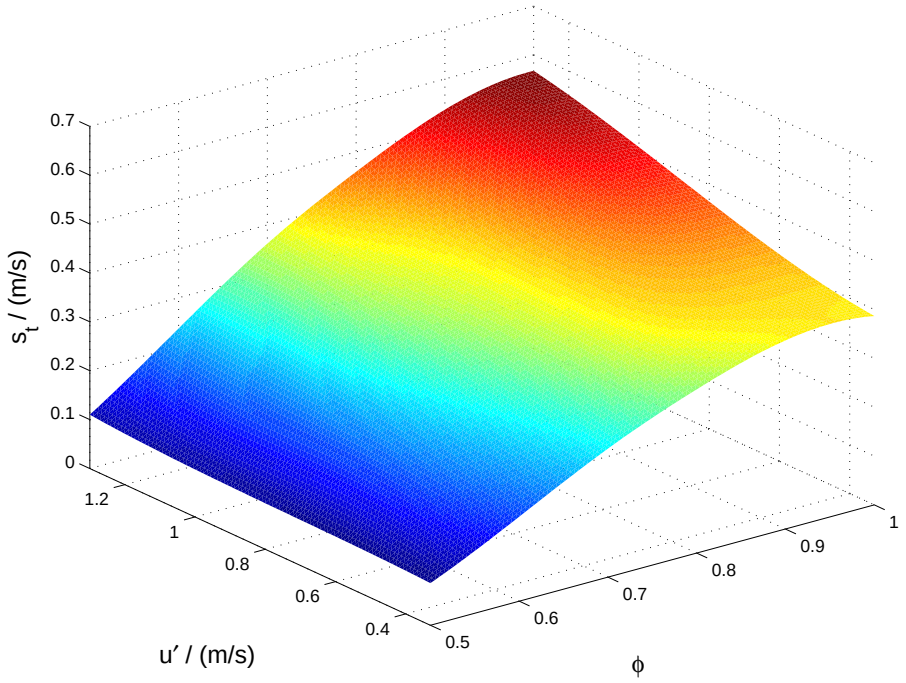

Figure 8: Tabulated turbulent burning speed as a function of stoichiometry and velocity fluctuations

these building blocks in detail. Since it is very difficult, if not impossible, to stabilize such a turbulent flat flame in an experimental setup, the method of choice for investigation is DNS. Compared to spherical flames the simulation of statistically stationary flat flames the simulation is more difficult since an inlet and an outlet boundary have to be defined. At the same time it represents a more physical situation, because practical appliances have an inlet for fuel intake and an outlet to emit exhaust gases. The geometry used in these studies is that of a statistically flat flame in a turbulent box. While per definition DNS resolves all turbulent scales, there are however some different choices for treating chemistry and boundary conditions, especially for turbulence. To make runtimes feasible often chemical reduction mechanisms are used. Another issue is how to maintain a given turbulent background state. We can summarize that results of DNS are not equal to other results of DNS without regarding these details.

De Swart et al. [8] investigate turbulent flame speeds with a DNS resolved flow field while using FGM for the chemical kinetics. A statistically flat flame is analyzed in a turbulent box. For this geometry the fully compressible Navier-Stokes equations are solved, as well as a conservation equation for the reaction progress variable. They used the scaled mass fraction of CO_2 as a reaction progress variable. In this case the GRI3.0 mechanism was used to generate the FGM database for this case of premixed methane/air at a stoichiometric ratio of $\phi = 0.7$. The simulation was initialized by a laminar incompressible flame solution which was superimposed on a three-dimensional turbulent field. The

turbulent field was created using random stream functions that were filtered and scaled to get the desired turbulent field. They consider decaying turbulence. The specific objective of their study was to shed more light on the flame-turbulence interaction, especially the influence of the small scale flow structures on local phenomena in the flame. This was done by analyzing turbulent mass burning rates.

The two configurations shown in Figure 7, named like in their original article, $C1$ and $C2$, lie in our tabulation zone. Therefore they are a good check for our turbulent flame speed results. The comparison is found in Table 4. The observed discrepancy between TFST and DNS results is about 20%. Since in the DNS decaying turbulence is considered, the observed time dependent flame speed is not quasi steady. It starts from the laminar value and reaches its maximum after order of a ms, but then decreases to relax back to the laminar state. However, this limit is not reached since the simulation time was only about two integral time scales. Under sustained turbulence conditions the quasi steady flame speed should hence be higher. So we interpret our overestimation of s_t as reasonable, but of course the comparison cannot be regarded as apples to apples since decaying turbulence is considered.

	C1 TFST	C2 TFST	C1 DNS	C2 DNS
l_t[mm]	2.78	2.78	2.78	2.78
l_F[mm]	0.556	0.556	0.556	0.556
$l_t/l_F[-]$	5.0	5.0	5.0	5.0
u'[m/s]	0.7	1.4	0.7	1.38
s_l[m/s]	0.216	0.216	0.213	0.213
$u'/s_l[-]$	3.3	6.5	3.3	6.5
$s_t/s_l[-]$	1.36	1.64	1.13	1.39

Table 4: Parameters and relations for DNS and TFST simulations

A second comparison is performed with another DNS of a freely propagating flame, this time under sustained turbulence conditions, taken from Chakraborty and Cant [3]. In the DNS a single-step Arrhenius type chemistry is used. Flames are analyzed in the thin-reaction-zone regime. Inlet and outlet conditions are specified, while the side boundary conditions are periodic. Inlet mass flow is varied until a quasi steady flat flame stabilizes.

TFST results are shown in Table 5 and compared to their DNS (case F of their paper) for equivalent non dimensional numbers relating turbulence and chemistry. This time we underestimate the DNS results by less than 10%.

	DNS Case F	TFST Case F
$l_t/l_F[-]$	4.05	4.05
$u'/s_l[-]$	7.62	7.62
$s_t/s_l[-]$	2.0	1.85

Table 5: Non dimensional relations for DNS and TFST simulations

Again, the steadiness of the DNS as well as of our runs is an issue to be consid-

ered. Looking e.g. at Figure 2b of the Chakraborty and Cant paper it becomes obvious that at the end of simulation they don't really reach a steady state after their simulation time of two integral turn over times. In the last quarter of the simulation the speed is rather 1.9 m/s (which is closer to our result) and attempts the 2.0 m/s compared with only at the end. We have noticed in our runs that even after 20 integral turn over times the mean value of s_t still is fluctuating. We have been far from a state were we reach strong convergence for the whole PDF(s_t). Of course current DNS studies are intended to yield a lot of statistical output. Nevertheless this output depends heavily on convergence, which is difficult to obtain in DNS, since the computations are very expensive.

We want to close this section with a comment on code performance. We see only a minor computational efficiency gain of FGM/LEM relative to detailed/LEM. The reason is explained in the following. Generally the speedup can be the same as reported in the literature [2] for FGM compared with detailed chemistry. This is also shown in section 7. However, our LEM code hasn't been tuned for speed at all and we are currently using a backward differencing (BDF) method for the time integrator in the turbulent runs. After LEM mapping events, the method has to be reinitialized, which is quite time consuming. This has to be done because each mapping event destroys the time history used by the BDF method. We plan to replace the integrator with another implicit method, that doesn't depend on old time steps. Such a method should carry over the same speed-up from the laminar to the turbulent case concerning the use of FGM instead of detailed chemistry.

5 TFST vs. an algebraic model

A first quantitative application of our new TFST idea over a broader parameter space than the DNS comparison is the interpretation of an algebraic model with relation to our turbulent flame speed results. We consider the turbulent flame speed model from [6] which has the following form:

$$s_t = s_l \left(1 + \min\left[\frac{\Delta}{l_F}, \Gamma \frac{u'_\Delta}{s_l}\right]\right)^\beta . \tag{7}$$

Here we set the filter size Δ to the integral turbulent length scales of the different runs and u'_Δ to the integral velocity fluctuations. The laminar burning velocities and the flame laminar thickness l_F are taken from the laminar flame calculations. Γ is an efficiency function defined in [6] and β a parameter associated with the fractal dimension of the turbulent flame surface. Here we will apply the model for our range of conditions and especially investigate the model's dependence on β. We consider an arbitrary choice of $\beta = 0.23$ which gives a fractal dimension of 2.23 and $\beta = 0.5$ which gives a fractal dimension of 2.5. In Figure 9 and Figure 10 the algebraic and TFST results are plotted over the parameter range under investigation. Whereas the agreement for the $\beta = 0.23$ case is quite good in the entire region, the results deviate from each other quite considerably for the $\beta = 0.5$ case at least in the high turbulence stiochiometric regions. In this limit an order one difference between the two models is observed. This illustrates the importance of the choice of the fractal dimension in the algebraic model. In the future it might be possible that our method helps to find reasonable choices for β depending on local turbulence/chemistry conditions.

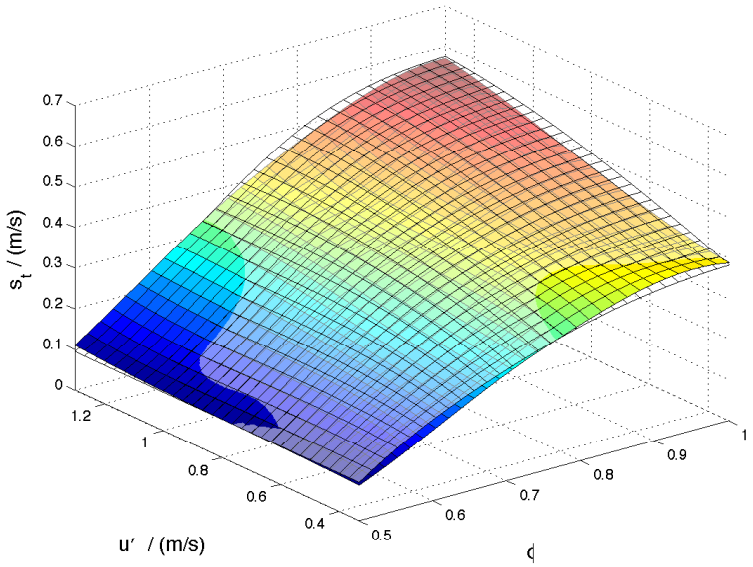

Figure 9: The turbulent burning speed s_t given by the algebraic model of Charlette for $\beta = 0.23$ (mesh) compared to TFST from Figure 8

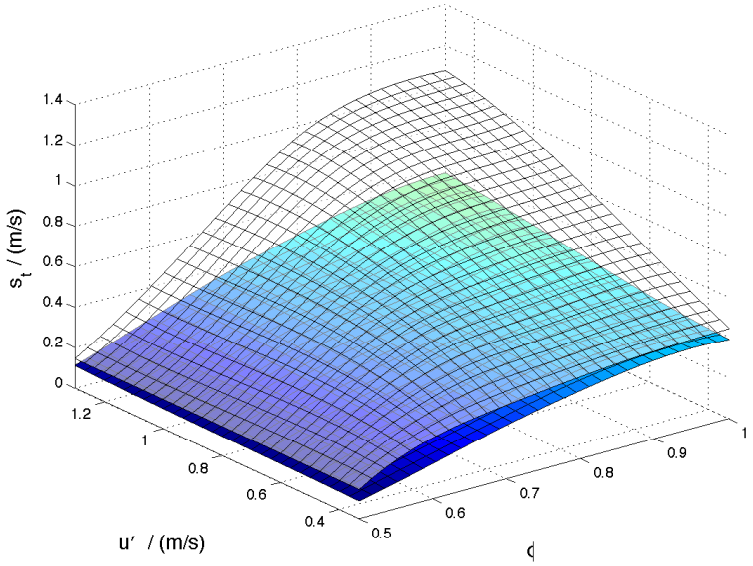

Figure 10: The turbulent burning speed s_t given by the algebraic model of Charlette for $\beta = 0.5$ (mesh) compared to TFST from Figure 8

6 An extension of the concept to strained flames

In this section we discuss an extension of TFST to incorporate effects of turbulent strain. A major issue in combustion is the relation of stretch to laminar

flame speed or consumption rate, see e.g. [7, 12] The local behavior of the stretched burning velocity s_l is observed to be taken into account already very well with DNS-FGM with a single progress variable Y_p and for $Le = 1$. So stretch effects change the profile of Y_p and this is sufficient to describe the change in mass burning rate and thus local laminar flame speed [2, 31].

While sections 2 and 3 show how to merge two well known models, the study of the notion of strain in LEM and FGM highlights a new, previously unexplored point. FGM inherently incorporates some strain effects as shown in [2, 31]. On the other hand, LEM has by definition of the triplet maps a qualitative view of the effect of strain. However, a quantitative description of strain in LEM is difficult. Therefore we propose the following extension:

1. We compute a set of stationary strained 1-D flames,
2. add to the FGM beside the progress variable Y_p an additional parameter, namely the absolute value of the gradient of the temperature, $|\nabla T|$, to characterize strain effects,
3. and finally search the chemical source terms in the LEM computation in the tabulated manifold with independent variables Y_p and its local gradient absolute value $|\nabla T|$.

In the first step, stationary laminar strained flamelets are computed and stored over the progress variable following the ideas of section 3.1. This means we solve again the one-dimensional zero-Mach-number equations using detailed chemistry. Strain is implemented via an additional spatially constant velocity gradient over the flame structure which alters the divergence constraint in the zero-Mach number formulation, equation (4), to

$$\begin{aligned} \frac{\partial u}{\partial x} &= -\frac{\partial v}{\partial y} - \frac{1}{\rho c_p T}\left\{\frac{\partial q}{\partial x} + \sum_s j_s \frac{\partial h_s}{\partial x}\right\} \\ &\quad -\frac{1}{\rho}\sum_s \left\{\frac{M}{M_s}\frac{\partial j_s}{\partial x}\right\} + \frac{1}{\rho}\sum_s \left\{\frac{M}{M_s} - \frac{h_s}{c_p T}\right\} M_s \dot{\omega}_s \end{aligned} \tag{8}$$

where $-\frac{\partial v}{\partial y}$ is a spatially constant strain rate imposed on the flame. Strain rates are varied systematically from zero to quenching conditions. Quenching was observed between strain rates of 13000 and 14000 $1/s$ for an equivalence ratio of 0.7. Sample snapshots of the source term of the progress variable are plotted in Figure 11. The strain imposed on the flame induces variations of the temperature gradient, as illustrated in Figure 12. Now, the key idea is to use ∇T as a parameterization of strain within the LEM concept.

In the second step, the incompressible one-dimensional Navier-Stokes equations supplemented by an equation for the progress variable are solved on a grid that resolves all turbulent scales (see section 3.2). Turbulent transport is implemented via LEM as before, but the triplet-map-induced gradients are now directly associated with the strain-induced gradients of the tabulated flamelets. In the standard method the source terms ω_i of species i are functions of the progress variable Y_p only. Here they are functions of instantaneous values of Y_p and ∇T. If gradients are locally increased by eddies, then the source terms directly feel this influence of turbulence, while in the standard method the chemistry would recognize it only by increased diffusion, but not as a direct effect on

chemistry. To our knowledge this is the first time that the triplet-map-induced folding which models the effects of compressive strain is directly associated with strain induced variations of the flame structure.

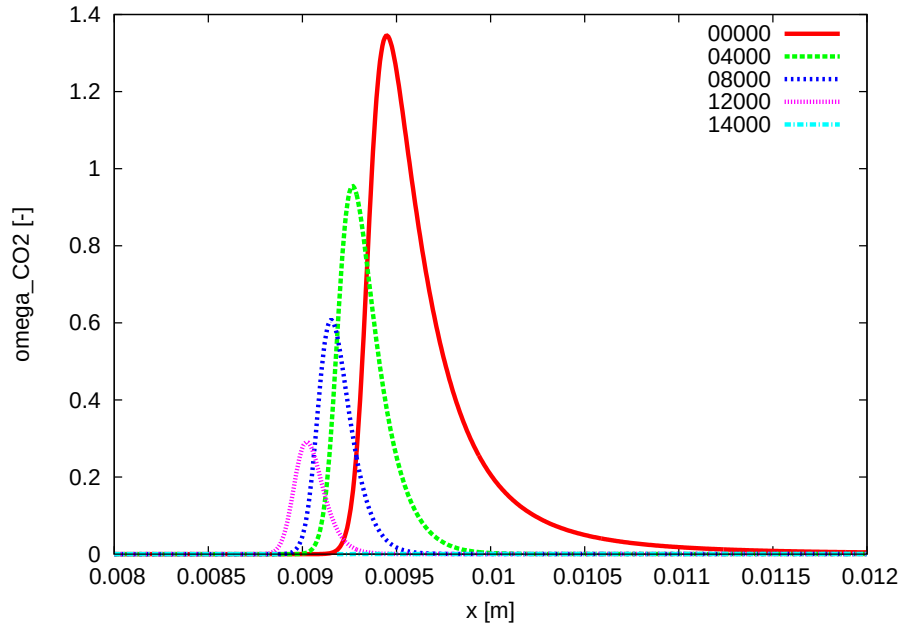

Figure 11: Effects of different strain rates in [1/s] on the source term of the progress variable CO_2 plotted over a part of the computational domain

To illustrate the extension of our concept to strained flames, we implemented it in a simplified fashion. For each strain rate we create an FGM data set and characterize the strain rate with the absolute value of the maximum gradient of T. The maximum gradient is always positive in the laminar 1-D flame used for table building, but both signs appear in the LEM computations. Hence, we use the absolute value to uniquely define the lookup position within the strained FGM database. Thus, for illustrating the concept we take $\dot{\omega}_i = f(Y_p, |\nabla T|_{max})$. This version is easier to implement and should show the capabilities of the method. Note that the triplet-map-induced local gradient is now directly associated with the strain-induced maximum gradient of the tabulated flamelets. This is surely oversimplified and could be extended in future work, e.g. one could search for local maxima of absolute values of gradients in the neighborhood of the point, where the source terms ω_i have to be evaluated. Results for the resulting steady gradients for the range of strain rates used are shown in Table 6. For a given local LEM value of $|\nabla T|$, the particular flamelet of Table 6 whose tabulation is interrogated to determine the full chemical state is chosen to be the one whose $|\nabla T|_{max}$ value is closest to the LEM $|\nabla T|$ value. In particular, for low, or zero, LEM $|\nabla T|$ values, the unstrained flamelet tabulation is interrogated. The extension to $\omega_i = f(Y_p, |\nabla T|)$ should be straightforward, but is more time consuming concerning the construction of the look up tables.

To show the effect of strain on the turbulent flame speeds we repeat the calculations (while keeping the integral scale fixed) and extend them as well to

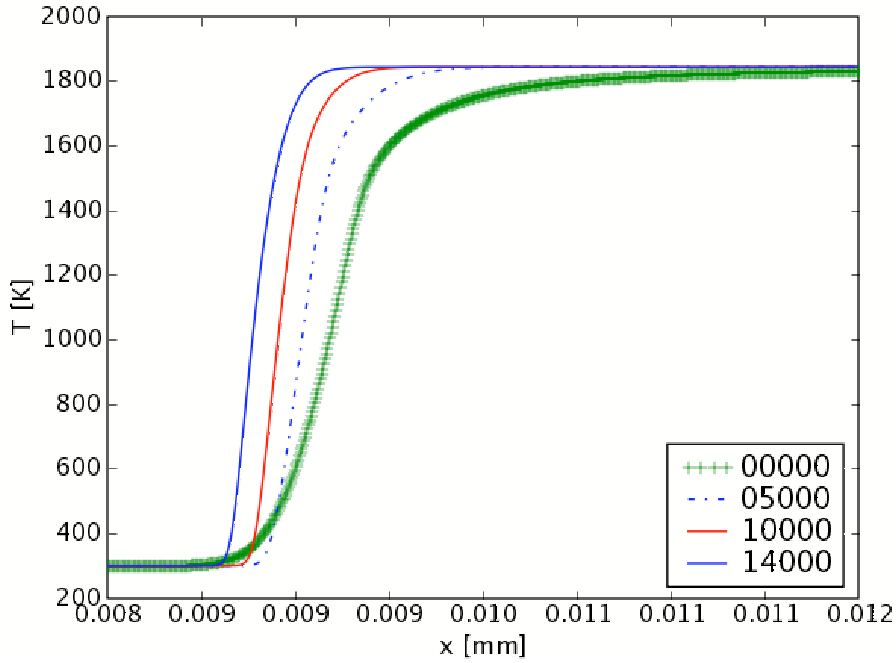

Figure 12: Structure of temperature, T, for different strain rates 0, 5000, 10000, and 14000 [1/s].

strain [1/s]	$\|\nabla T\|_{max}$	strain [1/s]	$\|\nabla T\|_{max}$
00000	5568	07000	9724
00500	5938	08000	10168
01000	6309	09000	10581
02000	6975	10000	10971
03000	7629	11000	11332
04000	8210	12000	11662
05000	8750	13000	11933
06000	9254	14000	11778

Table 6: Steady absolute value of maximum temperature gradient in [K/mm] for different strain rates

higher turbulent regions. The parameters and results are summarized in Table 7 and plotted in Figure 13. It can be seen that for weak turbulence conditions there is no difference in the mean flame speeds observable. Looking at the time series of $s_t(t)$ only after perturbations caused by LEM triplet maps minor changes in the strained and unstrained case are observable. The reasons for this are analyzed in more detail in the next section. For higher fluctuations one enters already into the broken reaction zone regimes and strain reduces the average burning speed. However, we have to mention that for the higher u' levels even the one dimensional computation is expensive. Especially for these cases we cannot claim at all convergence. In the future these cases have to

investigated in more detail. Nevertheless, looking at the time series for both cases one sees that strain really has an effect on s_t.

When accounting for $s_l = 0.216m/s$ for the Figure 13 case, the s_t/s_l values are an order of magnitude lower than in Peters [22] Figure 2.22. Fig. 13 is not comparable to the experiments for several reasons. Re_t varies with u' because l_t is held fixed (see Table 7) and the Re_t values are low except at the highest u' values. The highest u' values correspond to u'/s_l far higher than in the experiments. Nevertheless, the comparison suggests that s_t/s_l is quite small relative to the measurements. Of course, the LEM results are consistent with the DNS so this says that DNS also gives far smaller s_t/s_l than measurements. One consideration could be that l_t is $0.5cm$ in the LEM cases of Figure 13. Choice of small l_t reflects the small l_t in the DNS, which was presumably needed for affordable computations.

u'[m/s]	s_t[m/s]without strain	s_t[m/s]with strain	Re_t
0.33	0.263	0.263	23
0.66	0.301	0.301	46
0.99	0.341	0.341	69
1.30	0.362	0.362	92
2.60	0.461	0.461	185
5.20	0.663	0.654	371
10.40	0.774	0.749	728
20.80	1.029	0.988	1457

Table 7: The mean turbulent burning speed, s_t, for different u' calculated for $\phi = 0.7$, $l_t = 5mm$ with and without taking into account strain effects in the FGM tabulation.

7 FGM vs detailed chemistry under different flame structure perturbations

The flamelet generated manifold (FGM) technique is a powerful tool to reduce the parameter space in modeling turbulent combustion [29]. It has been tested as a reduction technique for direct numerical simulations (DNS), e.g. [31]. When we exchange tabulated against detailed chemistry for our turbulent simulations, only slightly different results for the mean of s_t were observed. A closer look at the time series (see Figure 6) nevertheless suggests that the two models behave (as expected) differently during unsteady phenomena like turbulent roll up and flame collision.

In the last section we obtained comparable trends, namely that the time series of s_t for strained and unstrained flames differ for a short time window when locally high strain rates (unsteadiness) are present.

Therefore in this section we investigate this scenario of high unsteadiness in a simplified way. We start again from a converged laminar flame profile and systematically add perturbations to the flame at different locations x_o and with different sizes l_{pert}. These perturbations mimic elementary roll up/collision scenarios in the well known combustion regimes. Each resulting perturbed laminar

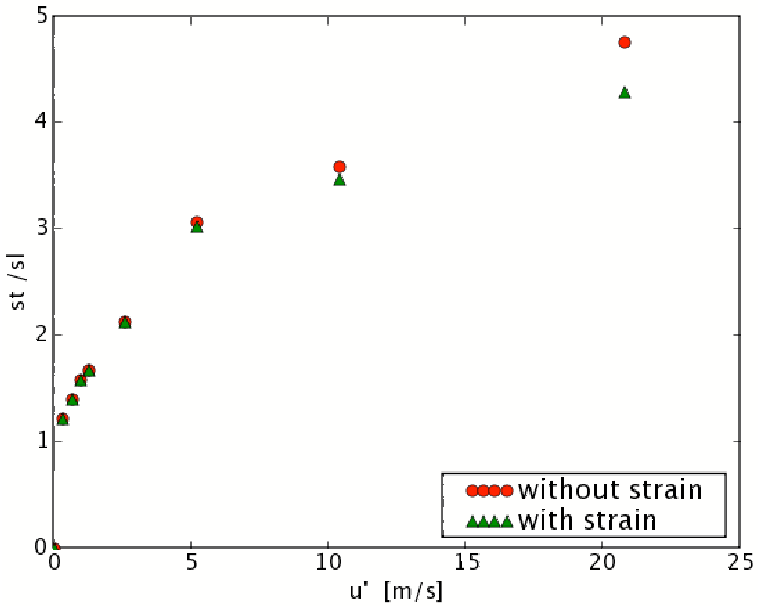

Figure 13: The mean turbulent burning speed, s_t, for different u' calculated for $\phi = 0.7$, $l_t = 5mm$ with and without taking into account strain effects in the FGM tabulation.

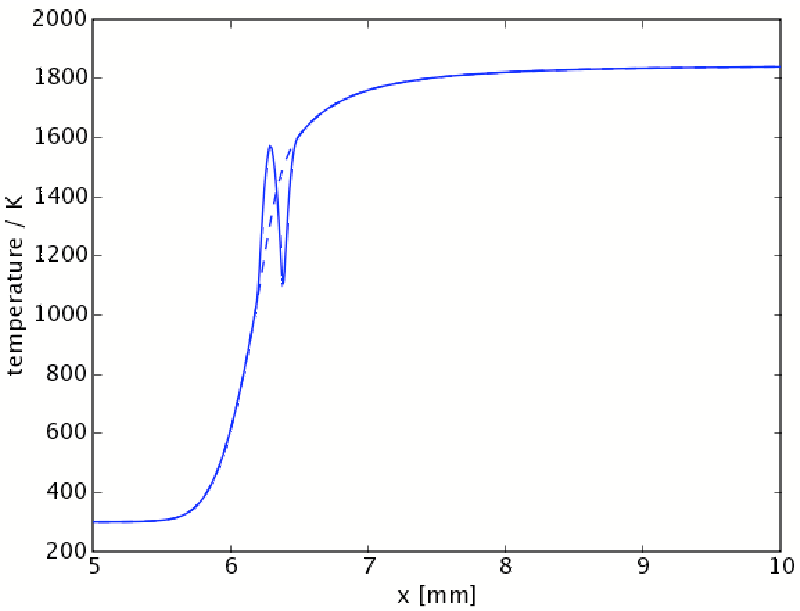

Figure 14: Initial flame temperature profile (dashed line) and a superimposed perturbation ranging from x_0 to $x_0 + l_{pert}$ (straight line)

flame, which is exemplified in Figure 14, is then used as an initial condition for one of our runs. Three different chemical models are used which are cou-

pled to an implicit solver for the one-dimensional Navier-Stokes equations [14]: (i) a detailed chemistry model, (ii) the standard FGM technique described in [29] using CO_2 as progress variable, and (iii) something we call a "redundant temperature case". The last case sounds heuristic, but could be interesting for LES subgrid scale models (SGS), as explained later. In this case we solve equation (3) for temperature during LEM time advancement and ignore the temperature solution stored in the FGM table. Now the source terms appearing in equations (3)-(5) are evaluated using this temperature and the tabulated species mass fractions, rather than using the tabulated source terms. The (iii) approximation accepts the CO_2 mass fraction as a reasonable representation of past history, but asserts that thermal transport not known by the table causes a *recent* change to temperature that should be communicated to the source terms. This captures the full nonlinearity of the source term concerning temperature. Note that case (iii) is not proposed as a new closure method, but it is obviously an option for people integrating FGM in an existing LES code, which of course solves for some temperature or total energy equation. For those users the performed test may help to estimate the consequences of ignoring the FGM stored temperature values. However, the more important comparison in this section is the one between detailed and classical FGM. Further note that here we are limited to 1D FGM rather than 2D FGM like in [30]. Therefore, one focus is the investigation of a whole set of turbulence scenarios rather than only one as done in a typical DNS study. A second issue is the study of the strain-dependent FGM based on the maximum gradient of T.

We consider a stationary laminar flame with a laminar flame thickness (measured by the steepest temperature gradient) of ≈ 0.55 mm and a reaction zone thickness of ≈ 0.15 mm measured with the CH_2O distribution. We chose three different perturbation length scales l_{pert} which give us typical scenarios in the flamelet regime (FR), the thin reaction zone regime (TRZR), and finally the broken reaction zone regime (BRZR). The perturbations are implemented via one single triplet map. In addition we varied the location of the perturbation. The 5.6 mm case induces a perturbation in the preheat zone, whereas in the other case the perturbation starts 0.6 mm shifted towards higher temperatures and has direct effect on the reaction zone. The setup is summarized in Table 8. Some representative results for the unsteady runs are plotted in the Figures 15 to 18. Figure 16 (case 2) and Figure 17 (case 5) show two runs with the same perturbation size, but different locations. The effect of the two cases on the time series of s_t is totally different. While in case 5 s_t is rising and later on relaxes to the initial state, in case 2 s_t first falls, then rises and relaxes to the steady state. Also the different chemical models behave differently. Generally the tabulated chemistry methods underpredict the decay and rise compared to the detailed chemistry. Concerning the transient behavior method (iii) predicts the amplitudes better than the classical FGM, but relaxes slower to the steady state than the two others.

In case 1 and case 4 (see Figure 15) the perturbation size is bigger, but the locations x_0 are the same as before. The two time series of s_t are comparable with the earlier observations, only the amplitude is higher as expected.

Finally, in Figure 18 (case 6) the perturbation size is only 0.11 mm. Again the locations x_0 for cases 3 and 6 are the same as before. The two time series of s_t show qualitatively the same behavior as for the other length scale perturbation sizes.

case	$l_{pert}[mm]$	l_{pert}/l_F	l_{pert}/l_R	FR	TRZR	BRZR	x_0 [mm]
1	1.1	2.0	7.0	X			5.6
2	0.275	0.5	1.75		X		5.6
3	0.11	0.2	0.7			X	5.6
4	1.1	5.0	7.0	X			6.2
5	0.275	0.5	1.75		X		6.2
6	0.11	0.05	0.7			X	6.2

Table 8: Table for the used perturbation locations and length scales and the associated non-dimensional numbers to simulate the typical case for the flamelet regime (FR), the thin reaction zone regime (TRZR), and the broken reaction zone regime (BRZR)

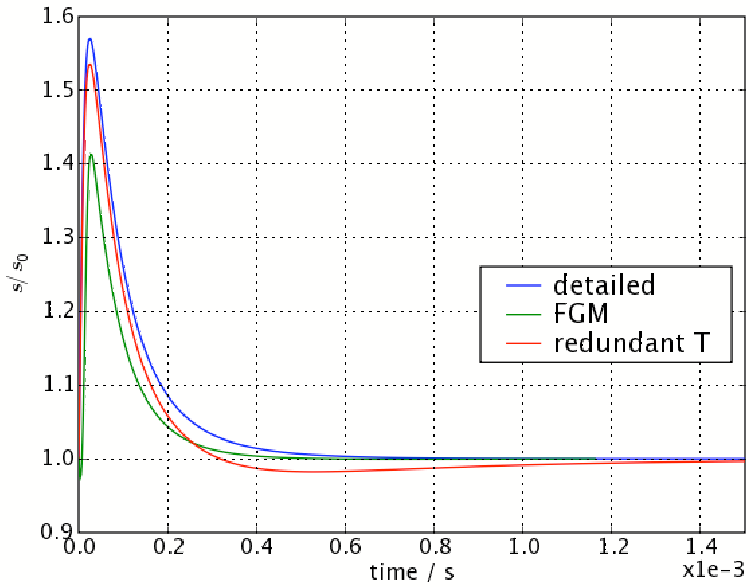

Figure 15: Time series of the normalized burning speed s. The computation starts with a perturbed steady laminar flame structure. The reaction zone is perturbed by an eddy of size 1.1 mm (case 4). The run ends when relaxation to a steady state is reached. The solutions for the three different methods used here are plotted.

In Table 9 we compare the normalized integral $\frac{1}{s_0(t1-t0)}\int_{t0}^{t1} s_l dt$ for the different cases. Here t_1 is the time after which s_l doesn't differ more than 1% from its starting value s_0 at t_0. This analysis gives a hint why FGM is still performing well in non-flamelet regimes. Considering cases 1, 2, and 3 with perturbations influencing the preheat zone alone (and not the reaction zone) we observe significant differences in s_t between the detailed chemistry and FGM calculations in cases 1-3. However, as can be seen from the figures, the deviation show both signs meaning that the time integral of the deviation vanishes (cancellation of errors). In contrast, the cases with perturbations influencing

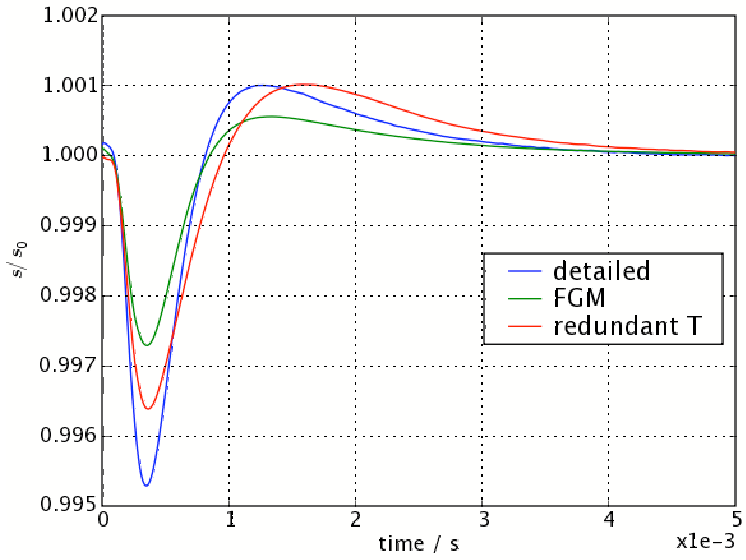

Figure 16: Time series of the normalized burning speed s. The computation starts with a perturbed steady laminar flame structure. The reaction zone is perturbed by an eddy of size 0.275 mm (case 2) and ends with the relaxation to a steady state. The solutions for the three different concepts are plotted.

the reaction zone for cases 4-6 show only deviations in one direction and no cancellation of errors occurs. This might be part of the reason why FGM has been successfully applied in the thin reaction zone limit where the underlying assumption of a steady flame structure is no longer fullfilled.

case	FGM	RedT	Det
1	1.022	1.052	1.029
2	1.000	1.000	1.000
3	1.000	1.000	1.000
4	1.058	1.058	1.033
5	1.005	1.008	1.008
6	1.0002	1.0006	1.0004

Table 9: Evaluation of the normalized dimensionless integral, $\frac{1}{s_0(t1-t0)} \int_{t0}^{t1} s_l dt$, for the cases 1-6 with a Simpson rule.

At the end we reconsider again the performance of our computations. The computational times relative to the detailed mechanism are summarized in Table 7. In these unsteady cases only a factor three in gain is seen using the tabulated chemistry. As said before we will consider and test other implicit solvers in future work.

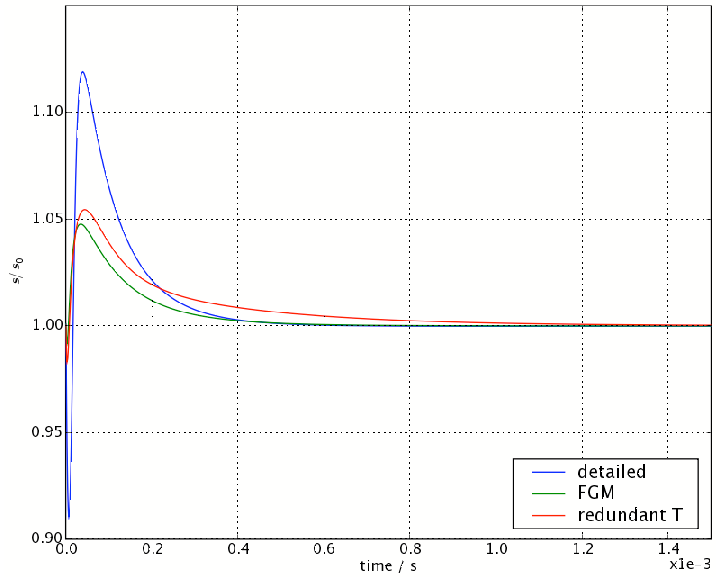

Figure 17: Time series of the normalized burning speed s. The computation starts with a perturbed steady laminar flame structure. The reaction zone is perturbed by an eddy of size 0.275 mm (case 5). The run ends when relaxation to a steady state is reached. The solutions for the three different methods used here are plotted.

case	cpu time FGM/det	cpu time RedT/det	cpu time det/det
1	0.36	0.33	1.0

Table 10: CPU times of the three methods in relation to the detailed chemistry for case 1

8 Summary and Outlook

An extended technique of an a priori turbulent flame speed tabulation (TFST) for a chosen parameter space is presented. In a first step, stationary laminar flamelets are computed and stored over progress variable following the ideas of flamelet generated manifolds (FGM). In a second step, the incompressible one-dimensional Navier-Stokes equations supplemented by the equation for the progress variable are solved on a grid that resolves all turbulent and chemical scales. In addition, turbulent transport is implemented via the linear eddy model (LEM). The turbulent flame structures are solved until a statistically stationary state for the mean flame speed is reached. The time for convergence is quite high compared with eddy turnover times. This is due to the fact that statistically rare events, like the big turbulent eddies, have a major impact on the flame structure and the burning speed. Only after a high number of these events the mean value converges. The results are stored in a table that could be used by large scale premixed combustion models, e.g. front tracking schemes.
First results are compared quantitatively with DNS results. Then we show how

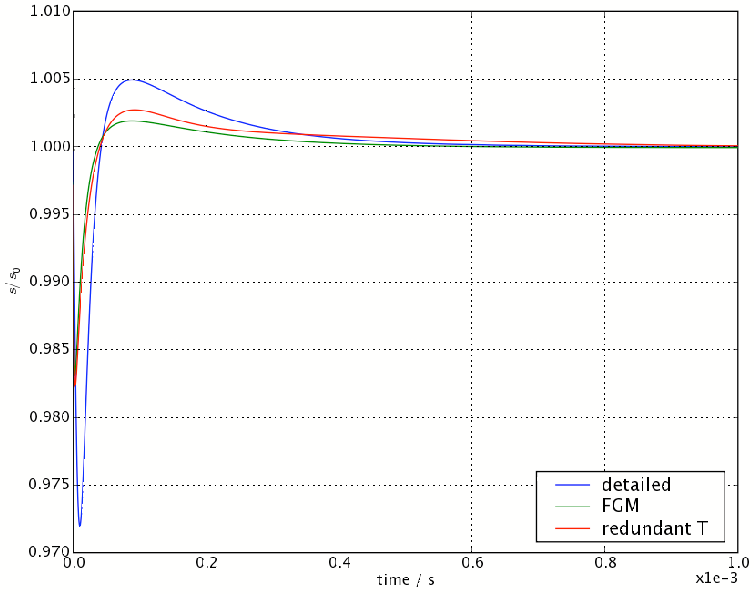

Figure 18: Time series of the normalized burning speed s. The computation starts with a perturbed steady laminar flame structure. The reaction zone is perturbed by an eddy of size 0.11 mm (case 6). The run ends when relaxation to a steady state is reached. The solutions for the three different methods used here are plotted.

our method might be used to evaluate the flame surface fractal dimension, a key parameter in a recent algebraic model for turbulent flame speed. Further it is shown how our technique can be extended to incorporate turbulent strain effects. At low turbulent intensity it was found that strain has no effect, whereas at high turbulence intensity there is some strain induced decrease in turbulent burning speed. Finally the effect of the use of detailed and tabulated chemistry under unsteady conditions was investigated. The effect of the perturbations was found to vanish after some time for all methods investigated. When the reaction layer is perturbed the return to steady state was observed to be relatively fast. We found that the tabulated chemistry is underestimating the deviations from the unperturbed mean state compared to detailed chemistry. However, for the cases where the perturbation were localized in the preheat zone the normalized integral of the burning speed over the perturbation time interval was comparable for the different types of methods. This could be an indicator why the schemes using tabulated chemistry still perform well in the thin-reaction-zone limit.
In the future, the idea can easily be extended to other parametric dependences of the turbulent burning speed. This could be, e.g, integral length scale effects. Our strategy could also be applied for building a PDF of subgrid scale (SGS) s_t values which could then be used in large eddy simulations (LES). The PDF can be built by averaging the LEM solutions over time intervals corresponding to LES time steps. Finally, the LES samples the s_t values from the constructed PDF. Justification of this procedure would require further investigation of the intermittent behavior discussed in Sec. 3.3.

ACKNOWLEDGEMENT

This work was partially supported by the Division of Chemical Sciences, Geosciences, and Biosciences, Office of Basic Energy Sciences, United States Department of Energy, and by the National Science Foundation under Grant No. ATM-0346854. Sandia National Laboratories is a multi-program laboratory operated by Sandia Corporation, a Lockheed Martin Company, for the United States Department of Energy under contract DE-AC04-94-AL85000. H. S. thanks the Deutsche Forschungsgemeinschaft (DFG) for partially supporting this work through grant SFB 557/B8. The authors gratefully acknowledge fruitful, stimulating discussions with J. A. van Oijen and L. P. H. de Goey.

References

[1] M.S. Anand and S.B. Pope. Calculations of premixed turbulent flames by pdf methods. *Combustion and Flame*, 67:127–142, 1987.

[2] R.J.M. Bastiaans, J.A. van Oijen, and L.P.H. de Goey. Application of flamelet generated manifolds and flamelet analysis of turbulent combustion. *Int. Jnl. Multiscale Comp. Eng.4(3), 307-317, (2006)*, 4(3):307–317, 2006.

[3] N. Chakraborty and R. S. Cant. Effects of strain rate and curvature on surface density function transport in turbulent premixed flames in the thin reaction zones regime. *Physics of Fluids*, 17:065108, 2005.

[4] V.K. Chakravarthy and S. Menon. Subgrid modeling of turbulent premixed flames in the flamelet regime. *Flow Turbulence and Combustion*, 65:133–161, 2000.

[5] V.K. Chakravarthy and S. Menon. Large-eddy simulation of turbulent premixed flames in the flamelet regime. *Comb. Sc. Techn.*, 162:175–222, 2001.

[6] F. Charlette, C. Meneveau, and D. Veynante. A power-law flame wrinkling model for LES of premixed turbulent combustion Part II: Dynamic formulation. *Combustion and Flame*, 131:181–197, 2002.

[7] L.P.H. de Goey and J.H.M. ten Thije Boonkkamp. A flamelet description of premixed laminar flames and the relation with flame stretch. *Comb. Flame, 119, (1999) 253-271.*, 119:253–271, 1999.

[8] J.A.M. de Swart, R.J.M. Bastiaans, J.A. van Oijen, and L.P.H de Goey. Turbulent burning rates from DNS of lean, statistically flat methane flames. In *Proc. of the European Combustion Meeting 2007, Chania, Crete*, 2007.

[9] O. Gicquel, N. Darabiha, and D. Thevenin. Laminar premixed hydrogen/air counterflow flame simulations using flame prolongation of ILDM with differential diffusion. *Proceedings of the Combustion Institute*, 28:1901–1908, 2000.

[10] G. M. Goldin. A-priori investigation of the constructed pdf model. *Proceedings of the Combustion Institute*, 30:785–792, 2005.

[11] D. Goodwin. Cantera: Object-oriented software for reacting flows. Technical report.

[12] D.C Haworth and T.J. Poinsot. Numerical simulations of lewis number effects in turbulent premixed flames. *J. Fluid Mech*, 244:405–436, 1992.

[13] J.C. Hewson and A.R. Kerstein. Stochastic simulation of transport and chemical kinetics in turbulent co/h2/n2 flames. *Comb. Theory Mod.*, 5:669–697, 2001.

[14] A. C. Hindmarsh. Sundials: Suite of nonlinear and differential/algebraic equation solvers. Technical report, UCRL-JRNL-200037, Lawrence Livermore National Laboratory, 2004.

[15] A. R. Kerstein. Linear-eddy model of turbulent transport and mixing. *Combustion Science and Techology*, 60:391–421, 1988.

[16] R.J. LeVeque. *Finite Volume Methods for Hyperbolic Problems*. Cambridge University Press, 2002.

[17] U. Maas and S. B. Pope. Simplifying chemical kinetics: Intrinsic low-dimensional manifolds in composition space. *Combustion and Flame*, 88:239–264, 1992.

[18] S. Menon and A.R. Kerstein. Stochastic simulation of the structure and propagation rate of turbulent premixed flames. *24th International Symposium on Combustion*, pages 443–450, 1992.

[19] M. Oevermann, H. Schmidt, and A. R. Kerstein. Linear eddy modelling of auto-ignition under thermal stratification with application to HCCI engines. In *Third European Combustion Meeting (ECM2007), Chania, Crete*, 2007.

[20] N. Peters. Fifteen lectures on laminar and turbulent combustion. Technical report, Ercoftac Summer School, RWTH Aachen, 1996.

[21] N. Peters. The turbulent burning velocity for large scale and small scale turbulence. *Journal of Fluid Mechanics*, 384:197–132, 1999.

[22] N. Peters. *Turbulent Combustion*. Cambridge University Press, 2000.

[23] R:. The r project for statistical computing. Technical report, http://www.r-project.org/.

[24] V. Sankaran and Menon. S. Structure of premixed turbulent flames in the thin-reaction-zones regime. *Proceedings of the Combustion Institute*, 28:203–209, 2000.

[25] V. Sankaran and Menon. S. Subgrid combustion modeling of 3-d premixed flames in the thin-reaction-zone regime. *Proc. Comb. Inst.*, 30:575–582, 2005.

[26] H. Schmidt and R. Klein. A generalized level-set/in-cell-reconstruction approach for accelerating turbulent premixed flames. *Combustion Theory and Modelling*, 7:243–267, 2003.

[27] T. Smith and S. Menon. Model simulations of freely propagating turbulent premixed flames. In *Proceedings of the Combustion Institute*, 1996.

[28] T. Smith and S. Menon. One-dimensional simulations of freely propagating turbulent premixed flames. *Combustion Science and Technology*, 128:99–130, 1997.

[29] J. A. van Oijen and L. P. H. de Goey. Modelling of premixed laminar flames using flamelet-generated manifolds. *Combustion Science and Technology*, 161:113–137, 2000.

[30] J.A. van Oijen, R.J.M. Bastiaans, , and L.P.H. de Goey. Low-dimensional manifolds in direct numerical simulations of premixed turbulent flames. *Proceedings of the Combustion Institute*, 31:1377–1384, 2007.

[31] J.A. van Oijen, R.J.M. Bastiaans, G.R.A. Groot, and L.P.H. de Goey. Direct numerical simulations of premixed turbulent flames with reduced chemistry: Validation and flamelet analysis. *Flow, Turbulence and Combustion*, 75:67–84, 2005.

[32] V. L. Zimont and A. N. Lipatnikov. A numerical model of premixed turbulent combustion of gases. *Chemical Physics Reports*, 14:993–1025, 1995.